Carbon, oxygen and biological productivity in the Southern Ocean in and out the Kerguelen plume :CARIOCA drifter results.

L.Merlivat, J. Boutin, and F.d'Ovidio

Sorbonne Universités (UPMC, Univ Paris 06)-CNRS-IRD-MNHN, LOCEAN Laboratory, 4 place Jussieu, F-75005 Paris, France

Abstract

Keywords: Biological productivity regime: in situ measurements- Carbon-Oxygen stoichiometry- Natural iron fertilization from the Kerguelen plateau- Iron control on carbon biological production- Phytoplankton blooms extending downstream.

The Kerguelen Plateau region in the Indian sector of the Southern Ocean supports annually a large-scale phytoplankton bloom which is naturally fertilized with iron. As part of the second Kerguelen Ocean and Plateau compared Study expedition (KEOPS2) in austral spring (Oct.-Nov. 2011), one Carioca buoy was deployed east of the Kerguelen plateau. It drifted eastward downstream in the Kerguelen plume. Hourly surface measurements of pCO_2, O_2 and ancillary observations were collected between 1st November 2011 to 12 February 2012 with the aim of characterizing the spatial and temporal variability of the biological Net Community Production, NCP, downstream the Kerguelen plateau, assess the impact of iron-induced productivity on the biological inorganic carbon consumption and consequently on the CO_2 flux exchanged at the air-sea interface.

The trajectory of the buoy until mid December was within the longitude range, 72°E-83°E, close to the polar front and then in the polar frontal zone, PFZ, until 97° E. From 17

November to 16 December, the buoy drifted within the Kerguelen plume following a filament carrying dissolved iron, DFe, for a total distance of 700km.

In the first part of the trajectory of the buoy, within the iron plume, the ocean surface waters are always a sink for CO_2 and a source for O_2, with fluxes of respective mean values equal to -8 mmol CO_2 $m^{-2}d^{-1}$ and +38 mmol O_2 $m^{-2}d^{-1}$. Eastward, as the buoy escapes the iron enriched filament, the fluxes are in opposite direction, with respective mean values of +5 mmol CO_2 $m^{-2}d^{-1}$ and -48 mmol O_2 $m^{-2}d^{-1}$. These numbers clearly indicate the strong impact of biological processes on the biogeochemistry in the surface waters within the Kerguelen plume in November-mid December, while it is undetectable eastward in the PFZ from mid-December to mid February.

While the buoy follows the Fe enriched filament, simultaneous observations of dissolved inorganic carbon, DIC, and dissolved oxygen, O_2, highlight biological events lasting from 2 to 4 days. Stoichiometric ratios, O_2/C, between 1.1 and 1.4 are observed indicating new and regenerated production regimes. NCP estimates range from 60 to 140 mmol C $m^{-2}d^{-1}$.

1 Introduction

The Southern Ocean is a key region for the global carbon cycle and the climate system. It accounts for about 25–30% of the anthropogenic carbon uptake by the ocean. The Southern Ocean (south of about 30°S) is found to be a sink area for atmospheric CO_2 in atmospheric or ocean inversion models (Friedlingstein et al., 2006; Gruber et al., 2009) as well as in data based approaches (Metzl et al., 1999; Takahashi et al., 2009). However, it represents a sink for atmospheric CO_2 whose strength and future evolution are debated (Le Quere et al., 2010, Lenton et al., 2013). Despite its importance, the Southern Ocean remains the region where uncertainties regarding the air–sea CO_2 flux and the carbon budget are the highest (e.g., Gruber et al., 2009). This remote part of the global ocean is hardly accessible in winter, leading to a very sparse spatiotemporal coverage of observations, including measurements of surface pCO_2. Undersampling biases are aggravated by the high variability which characterizes this oceanic region over a wide range of temporal and spatial scales. Quantification of the impacts of thermodynamics, biology, and physics on the sea surface partial pressure of CO_2, pCO_2, is a necessary step to understand the processes regulating the ocean–atmosphere exchange of CO_2 and help to overcome the unresolved spatio temporal variability effects.

The magnitude of the gradient of pCO_2 between the atmosphere and the surface ocean depends on the relative contribution in the ocean mixed layer of the dynamic transport, the thermodynamics and the biological activity. Biological net community production, NCP, decreases sea surface pCO_2. In high nutrient-low-chlorophyll, HNLC, regions, including the Southern Ocean, more than two decades of intense research have confirmed that increasing iron supply stimulates primary production. (Boyd et al, 2007, Blain et al, 2008). Large and persistent phytoplankton blooms develop annually in the vicinity of sub-Antarctic islands (Blain et al., 2007; Borrione and Schlitzer, 2013; Pollard et al., 2009) due to natural iron supply. The results of field studies in the vicinity of Crozet and Kerguelen islands have clearly highlighted the crucial role of Fe on natural ecosystems and demonstrate the stimulation of the biological carbon pump. In February 2005, the KErguelen Ocean and Plateau compared Study expedition, KEOPS1, focused on the high productivity area of the Kerguelen Island during the peak and decline of the bloom (Blain et al, 2007). The results emphasized the opportunity of studies on the Kerguelen plateau to investigate the functioning of the biological carbon pump in a naturally iron-fertilized region. The KEOPS2 project in October-November 2011, designed to improve the spatial and temporal coverage of the Kerguelen region, was carried out in austral spring to document the early stages of the bloom and to complement results of KEOPS1.

As part of KEOPS2 a CARIOCA buoy has been launched, drifted eastward close to the polar front then entered the polar frontal zone, PFZ. NCP is deduced from high frequency pCO_2 measurements made in November-December along the trajectory of the drifter. The aim of the present work is to provide a zoom on the extent of the iron seeding downstream the plateau during the end of the spring, its effect on the production of organic carbon and its control of the CO_2 air-sea flux

2 Data and methods

2.1 Site description

A Carioca buoy was deployed as part of the KEOPS2 expedition that took place from 9 October to 29 November 2011, in the Indian sector of the Southern Ocean in the vicinity of the Kerguelen archipelago. It was deployed on 1st November 2011 over the Kerguelen plateau and drifted eastward downstream within the Kerguelen plume. Until 12 February 2012, its ~1800 kilometers long trajectory followed the polar front closely, entering the polar frontal zone on the 16 December 2011(figure 1). The buoy acquired data in the 72°E-75°E longitude range of the intensive KEOPS 2 field campaign from 1st to 15 November 2011 and then was advected downstream within the Kerguelen plume later in the season.

2.2 Buoy measurements

The Carioca buoy was equipped with a CO_2 sensor (Copin-Montegut et al., 2000; Hood and Merlivat, 2001) and an Anderaa F3835 optode to measure dissolved O_2 (Lefevre and Merlivat, 2012).The partial pressure of CO_2, pCO_2, dissolved oxygen concentration, O_2, sea surface temperature, SST, and sea surface salinity, SSS, were measured at a depth of 2 meters on an hourly basis. Atmospheric pressure and wind speed are measured at a height of 2 meters, which were subsequently corrected to 10 meters height values. Collected data have been transmitted by the buoy in real time via the Advanced Research and Global Observation Satellite (Argos) data network.

Strictly, the CO_2 sensor measures the fugacity of CO_2, fCO_2, which is not identical to pCO_2 owing to the non-ideal nature of the CO_2 gas (Dickson et al, 2007). In the range of SST of our study, the difference between pCO_2 and fCO_2 is close to 1.4 μatm, which is within the instruments 3 μatm absolute error. Accordingly, we will approximate fCO2 as being equal to pCO_2 within this study.

Alkalinity, Alk (μmol kg^{-1}), is computed from SST and sea surface salinity, SSS, using the alkalinity-temperature-salinity relationship proposed by Lee et al. (2006) for the Southern Ocean. Dissolved inorganic carbon, DIC (μmol kg^{-1}), is derived from pCO_2, Alk, SST and SSS using the CO_2 dissociation constants of Mehrbach et al. (1973) as refitted by Dickson and Millero (1987) and solubility from Weiss (1974). An accuracy of 10.5 μmol kg^{-1} was estimated, as a result of the combined uncertainties linked to the dissociation constants, the accuracy of pCO2 measurements and the uncertainty of the alkalinity derived from the relationship proposed by Lee et al. 2006 (Boutin et al, 2008). The relative precision of successive DIC values is expected to be 0.5 μmol kg^{-1} (Boutin et Merlivat, 2009, Merlivat et al, 2014).

The oxygen optode measurements were calibrated initially in the laboratory prior to deployment using a zero and 100% oxygen reference points. During the KEOPS 2 cruise, the optode data were subsequently calibrated against the oxygen Winkler measurements made with an accuracy of 0.2% (D.Lefèvre, personal communication). A constant offset of 13.6 μmol kg^{-1} between the two techniques was found. Johnson [2010] compared the optode measurements recorded at a time series off Monterey Bay, California, with shipboard measurements made using the Winkler method. He found an offset between the two techniques, which remained constant over the 5 months period of his record Therefore, we simply apply an offset of 13.6 μmol kg^{-1} to correct the optode data. Oxygen saturation, O_{2sat} (in μmol kg^{-1}) is calculated using the equation of Garcia and Gordon (1992). The degree of O_2 saturation, (in percent), is given by:

$$\%\ O_2\ sat = ([O_2] / [O_2^{sat}])\ x100$$

2.3 Calculation of air-sea fluxes of CO_2 and O_2

The hourly air-sea CO_2 flux, F_{CO2} (mmol m^{-2} d^{-1}), is derived from wind speed, the air-sea gradient in pCO_2 and the gas transfer velocity [Boutin et al., 2008; Merlivat et al, 2014], following:

$$F_{CO2} = k_{CO2}\ \alpha_{CO2}\ (pCO_{2sea}-pCO_{2atm}) \qquad (1)$$

where α_{CO2} is the solubility of CO_2 (Weiss, 1974), pCO_{2sea} the partial pressure of CO_2 in seawater (μatm), pCO_{2atm} the partial pressure of CO_2 in the atmosphere (μatm), and k_{CO2} (cm/h) is the gas transfer velocity for CO_2. pCO_{2atm} is computed from the monthly molar fraction xCO_2 at the Macquarie Island atmospheric station (NOAA/ESRL Global Monitoring

Division (http://esrl.noaa.gov/gmd/ccgg/iadv)), the water vapor pressure of Weiss and Price (1980) and the atmospheric pressure recorded on the drifter.

Injection of air bubbles below the air-water interface is neglected for the calculation of the CO_2 flux but this contribution to the flux can be relatively important for oxygen. The equation of the O_2 flux is then given by:

$$F_{O2} = k_{O2} ([O_2]-[O_{2sat}]) - F_{bub} \qquad (2)$$

where k_{O2} is the gas transfer velocity for O_2 and F_{bub} is the contribution of air bubbles using the formula given by Woolf and Thorpe (1991):

$$F_{bub} = k_{O2}\, 0.01(U/U_0)^2 [O_{2sat}] \qquad (3)$$

with U the wind speed at 10m height in ms^{-1} and U_0 a model-derived constant wind speed value equal to 9 ms^{-1} to compute bubbles O_2 air-sea flux.

. The total oxygen flux becomes:

$$F_{O2}=k_{O2} ([O_2]-[O_{2sat}] (1+1.23\ 10^{-4}U^2)) \qquad (4)$$

It results from this equation that the flux is positive when there is outgassing to the atmosphere.

For both CO_2 and O_2, the gas transfer velocity is calculated using the formula of Sweeney et al. (2007):

$$k = 0.27\ U^2(660/Sc)^{0.5} \qquad (5)$$

where Sc is the Schmidt number, Sc_{CO2}, for CO_2 or Sc_{O2} for O_2 (Wanninkhof, 1992) and U the 10m wind speed .

2.4 Calculation of in-situ Carbon and Oxygen biological production

Net community production, NCP_C, has been previously derived from drifting CARIOCA buoys measurements, by looking at day-to-day evolution of DIC at dawn provided that daily cycles of DIC in phase with the ones expected from biological activity are observed (Merlivat et al, 2009, Boutin and Merlivat, 2009; Merlivat et al, 2014). In addition, in case O_2 is measured, it is possible to simultaneously estimate NCP from O_2 day-to-day evolution, NCP_{O2} (Lefèvre and Merlivat, 2012). The method relies on hourly measurements of SST, SSS, pCO_2 and O_2 to estimate in-situ biological production from unattended platforms using a non-intrusive method. During the daylight period, photosynthesis, respiration, and air-sea exchange are mechanisms responsible for the change in DIC and O_2 recorded at 2m depth. If no significant change in salinity is observed, the processes of advection and mixing, and thus DIC and O_2 fluxes through the base of the mixed layer, h, are assumed to be negligible. Depending on atmospheric forcing, a warm diurnal layer, h*, can form during daylight (Merlivat et al., 2009). In this surface layer, of depth h*, from sunrise to sunset, due to combined effect of photosynthesis and respiration, DIC generally decreases and O_2 generally increases; they reach minimum, DICmin, and maximum, O_2max, values at the end of the day. At night, as a result of respiration and of the mixing between the warm layer and the mixed layer, DIC increases and O_2 decreases; they reach maximum, DIC max, and minimum, O_2 min,values at the end of natural convection. NCP is derived from day-to-day change of DICmax and O_2min, after removing the contribution of the air-sea fluxes. Contribution of biological activity (photosynthesis plus respiration) during daylight is derived from DICmax-DICmin, and O_2min-O_2max after removing the contribution of the air-sea fluxes. Figure 2 shows SST, DIC and O_2 over a 4 days period, 30 November-4 December 2011. The mean increase of SST equal to 0.044°C d^{-1}, superimposed on daily cycles of SST, indicates a stratification of the mixed layer over this 4 days period. No change of salinity is measured (not shown). Thus, the changes in DIC and O_2 observed during the 4 days were only driven by biological processes allowing the computation of NCP. The carbon and oxygen mass balance, either in the daytime interval during the development of the warm layer, h*, or over one day time interval in the mixed layer, h, result in the two following equations:

$$\left(\frac{\Delta DIC}{\Delta t}\right)_{measured} = \left(\frac{\Delta DIC}{\Delta t}\right)_{bio} + \left(\frac{\Delta DIC}{\Delta t}\right)_{air-sea} \quad (6)$$

$$\left(\frac{\Delta O_2}{\Delta t}\right)_{measured} = \left(\frac{\Delta O_2}{\Delta t}\right)_{bio} + \left(\frac{\Delta O_2}{\Delta t}\right)_{air-sea} \quad (7)$$

NCP integrated over the mixed layer is given by:

$$NCP_C = \rho h \frac{\Delta DIC_{max}}{\Delta t} + F_{CO_2} \quad (8)$$

$$NCP_{O_2} = \rho h \frac{\Delta O_{2min}}{\Delta t} + F_{O_2} \quad (9)$$

where F_{CO2} and F_{O2} are the air-sea CO_2 and O_2 flux (mmol m^{-2} d^{-1}), positive when there is outgassing to the atmosphere. h (m) is the depth of the mixed layer, ρ (kg m^{-3}) is the density of seawater and $\Delta DIC_{max}/\Delta t$ and $\Delta O_{2min}/\Delta t$ (µmol $kg^{-1}d^{-1}$) are the change of DIC (and O_2) between two consecutive maxima (and minima).

Between two consecutive mornings, at the end of nocturnal convection, $dDIC/dt_{air-sea}$ and $dO_2/dt_{air-sea}$ are equal respectively to F_{CO2}/h and F_{O2}/h, (where h is the mixed layer depth). During the daily stratification period, the diurnal mixed layer thickness decreases from h to h* when DIC is minimum and O_2 is maximum. We make the assumption that it varies linearly from h to h* in order to compute the hourly values of the air-sea flux contribution, $(F/h)_i$, which then are added over the daily stratification period. We assume that the minimum depth of the diurnal mixed layer, h*, at the end of the production period is equal to the sampling depth 2m. A mixed layer depth equal to 20 m has been adopted based on observations made during the KEOPS 2 field campaign under conditions similar to those encountered by the buoy. We will discuss later the uncertainties related to this choice.

2.5 Chlorophyll and age distribution of the water parcels over and downstream of the Kerguelen plateau

The time and spatial changes of the phytoplankton bloom as revealed by satellite ocean color are shown in figure 3 (on which the buoy trajectory is indicated). The strongest bloom is observed from 11 November to 2 December, about two months after bloom initiation, followed by a clear decay early summer in December.

The horizontal transport of water parcels eastward of the Kerguelen plateau has been derived from altimetry (d'Ovidio et al 2015). From this analysis, the time since a water parcel has left the plateau (so called age of the water parcel) could be estimated. The trajectory of the Carioca buoy was placed in this temporal framework using the age map of 25th November (figure 4). Over the period 1st November to 31 December, the buoy has sampled a large range of water parcels with different ages as shown by the stirring pathways east of the Kerguelen plateau close to the trajectory of the drifter. NCP estimates have been made over the period 18 November-13 December (Tables 1 and 2).

3 Results

3.1 Buoy measurements

The variations of SST and SSS observed along the trajectory of the buoy are largely explained by its position relative to the polar front, PF (figure 1). From 1st to 12 November, the buoy was drifting in the meander of the PF (Park et al, 2014) with SST~3°C and SSS ~33.83. From 12 November to 16 December, while the buoy followed closely and sometimes crossed the PF, SST is ~4.2°C and SSS ~33.75. During this time interval, simultaneous short time peaks of SST (negative) and SSS (positive) were observed whilst transiting the PF (figures 1 and 5a). From 16 December 2011 to 11 February 2012, the buoy drifted in the polar frontal zone, where higher temperature (close to 6°C) and higher salinity, (in the range 33.8 to 33.9) were measured.

A very large variability of pCO_2 values, from ~280 μatm to ~400 μatm, are observed while the buoy is drifting in the meander of the PF (figure 5c). Shipboard measurements of pCO_2 made during the KEOPS 2 field campaign show a similar range of variability (Lo Monaco et al, 2014). During periods when the buoy is southward or close to the PF, the surface waters are undersaturated in CO_2 relative to atmospheric CO_2. After 17 December, in the polar frontal zone, the surface waters become supersaturated. Moreover, the surface waters are supersaturated in oxygen until 16 December, with saturation values up to 110% (figure 5d). In the polar frontal zone, data showed O_2 undersaturation

3.2 Air-sea flux of CO_2 and O_2

From 1st November to 17 December surface waters are a source of O_2 (figure 6a) for the atmosphere and a sink of CO_2 (figure 6b). Conversely, in the polar frontal zone, east of 83°E, we observe an ingassing of O_2 and outgassing of CO_2. It is worth noting that the absolute values of the fluxes are larger for O_2 than for CO_2 due to the buffer factor of ocean water carbonate chemistry. From 1st November to 16 December, the flux of O_2 and CO_2 are respectively 38±34 mmol $m^{-2}d^{-1}$and -8.3±7.5 mmol $m^{-2}d^{-1}$. After 16 December, they are equal respectively to -48±43 mmol $m^{-2}d^{-1}$ and 5.3±4.7 mmol $m^{-2}d^{-1}$.

3.3 Dissolved inorganic Carbon, DIC, and oxygen

A significant reduction in DIC of ~ 50μmol kg^{-1} is observed from November 1st to December 17th, followed by an increase of approximately 20 μmol kg^{-1} when the buoy crossed the PF and starts drifting northward in the polar frontal zone. At the same time, a sharp decrease of the O_2 concentration is measured (figure 7). During the first part of the trajectory of the buoy close and along the PF, the highly variable distribution of the concentrations of DIC and O_2 are controlled by physical transport processes, lateral advection and vertical mixing, air-sea exchange, and biological processes. Four periods for DIC and O_2 of 3 to 5 days have been identified when only air-sea exchange and biological processes control the change with time of the concentrations of DIC and O_2, as described by equations 6 and 7 (cf. also figure 2). For 7 days during these periods, the amplitude of the difference between the extrema (|Max-min|) for DIC and O_2 in the warm daily surface layer, h*, have been measured (table 1 and figure 8).

3.4 Quantification of biological processes

Large amplitudes of the diurnal cycles of DIC and O_2 up to 12 µmol kg^{-1} have been measured, while day-to-day changes peak at 5 µmol kg^{-1} (figure 8). These numbers represent the contribution of the biological processes plus the air-sea exchange terms (equations 6 and 7). Their ratio is close to one (figure 8). In table 1, it is interesting to note the wide range of values of CO_2 and O_2 air-sea fluxes, the O_2 fluxes being up to 6.6 larger than the CO_2 ones.
A summary of the biological and air-sea flux terms for DIC and O_2 is given in table 2. Figure 9 shows the simultaneous biological changes of O_2 and DIC observed in the ten selected situations. The DIC measurements are used to calculate NCP_C (equation 8 and table 2). In November, 2 values of NCP_C respectively equal to 140±7 and 124±23 mmol C $m^{-2}d^{-1}$ are computed. In December, we have NCP_C equal to 60±12 and 72±17 mmol C $m^{-2}d^{-1}$. The standard deviation does not include the uncertainty on the choice of the value of the MLD.

4 Discussion

4.1 Hydrodynamical environment along the trajectory of the buoy

During the 2011 KEOPS2 cruise, Park et al (2014) determine and validate an up-to-date location of the PF around the Kerguelen Islands over the longitude range, 68°E-78°E. The PF, defined as the northern limit of the subsurface minimum of temperature, T_{min} of 2°C, was validated based on in-situ hydrographic and current measurements made during the cruise, satellite ocean color images, and altimetry-derived surface velocity fields. The PF location rounds the Kerguelen Islands from the south, executing a permanent cyclonic meandering in the off-plateau area immediately east of the Kerguelen Islands until the longitude of 73.5°E, then extends eastward (figure 5, Park et al, 2014).

The buoy, after drifting inside the meander, traverses the front many times during which rapid increases of salinity are observed (figures 1 and 5). Eastward of 78°E, the comparison of the two routes cannot be so specific as the trajectory of the buoy is compared with a large scale climatological PF (Park et al, 2009, 2011) which certainly does not take into account the highly time-varying frontal circulation of the area. On 16 December, the latitude of the polar front as derived from the buoy measurements (figures 1 and 5) is very close to the climatological PF.

4.2 Lagrangian distribution of chlorophyll along the trajectory of the buoy

The sequence of ocean color images on which is superposed the trajectory of the buoy from 11 November to 28 December (figure 3) show the rapid development of the bloom until 2 December and then its decline. In most cases, the buoy follows the highly time-varying mesoscale meanders observed within satellite chlorophyll images. In their detailed study of the location of the PF during the KEOPS 2 cruise, Park et al (2014) put forward that the high-resolution chlorophyll concentration images appear as an excellent marker of the fronts and filaments, supporting evidence for the frontal circulation determined from the combined hydrography, altimetry, and drifters tracking data. We then are led to conclude that the biological processes identified during 4 periods along the trajectory of the buoy (figure 1 and table 1) are representative of frontal conditions which favor biological production. Specifically, the data computed between 18 to 28 November, in the longitude domain 76°E-78°E, seem very tightly linked to the complex structures of the PF (figure 1).

In figure 4, the trajectory of the buoy is superposed on a mapping of the age of the water parcels since they have left the plateau where they are loaded with iron (d'Ovidio et al., 2015). The rate of change of the horizontal dissolved iron supply, DFe, downstream the plateau is modeled with an exponential decay of the initial on-plateau iron stock in the water column.

The data in figure 4 can be interpreted as representative of the changes of the stock of DFe in the ocean upper layer (0-150m), the largest DFe concentrations in the youngest waters. It is interesting to emphasize, at least qualitatively, the relationship between the distribution of DFe and the signature of the biology on the DIC and O_2 concentrations measured along the trajectory of the buoy. As a first example, when the buoy escapes the rich DFe waters on 15-16 November (the cyan square in figure 4) large abrupt changes of DIC (an increase) and O_2 (a decrease) are observed (figure 7), suggesting the lack of organic matter production in the absence of iron.

4.3 Carbon and oxygen biological production regimes

During the KEOPS 2 expedition, MLD were estimated at 3 stations (TEW-7, TEW-8, F-L) very close to the PF (Park et al, 2014), (figure 1). The average MLD at these stations, calculated with the criteria: depth where the potential density = potential density at 10 m + 0.02 kg m^{-3}, was equal to 20 m (Park et al., 2014, Trull et al, 2015). We elect to use this depth as our MLD definition, as physical (T, S) characteristics at these stations are very similar to CARIOCA measurements (figure 5b). Furthermore, the choice of a relatively shallow mixed layer, 20 meters, is supported by the work of Taylor and Ferrari (2012) who found, based on numerical simulations, that restratification at fronts can inhibit vertical mixing, triggering high latitude phytoplankton blooms. However, the values of NCP integrated over the depth of the mixed layer may be an underestimate if the depth of the euphotic layer, Ze, is greater than MLD. During the KEOPS 2 expedition at the station F-L, Cavagna et al (2014), indicate Ze=30meters. From the vertical profile of net primary production, NPP, based on the analysis of carbon 13 incubation experiments, the computed value of NPP integrated over 20 meters represents about 75% of NPP integrated over Ze. NPP at depth greater than Ze is negligible close to 2%. We take into account an underestimation of 33% to compute NCP, as the euphotic layer depth is larger than the MLD which is equal to 20 meters.

The values of the carbon net community production, NCP_C, which corresponds to DIC transformed into particulate organic carbon, POC and dissolved organic carbon, DOC by biological activity, vary from 130 mmol $m^{-2}d^{-1}$ between 23 and 28 November and then decreases to about 65 mmol $m^{-2}d^{-1}$at the beginning of December (table 2). A similar range of values of carbon net community production along fronts in the Southern ocean have previously been observed (Merlivat et al, 2014). During the KEOPS 1 expedition in 2005, Lefevre et al (2008) and Jouandet et al (2008) measured NCP at 2 stations south of the polar front. At the same locations, NCP measured at a five days interval varies between 105 and 43 mmol C m^{-2} d^{-1}. This illustrates the large spatial and temporal variability of processes which control NCP, depending on the bathymetry and the physical and dynamical regime prevailing in the upper layers in the KEOPS 2 field study

The biological terms, $\left(\frac{\Delta O_2}{\Delta t}\right)_{bio}$ and $-\left(\frac{\Delta DIC}{\Delta t}\right)_{bio}$ are represented on figure 9 on which the 2 lines with slopes equal to 1.4 and 1.1 indicate the expected oxygen-carbon relationship respectively for a new production regime (photosynthetic quotient, PQ=1.4) or a regenerated one, PQ= 1.1, (Laws, 1991), During daytime, DIC and O_2 variations represent GCP-R/2 (GCP, Gross Community Production, R, Respiration) if we assume the respiration rate constant over a day. From dawn to dawn, it corresponds to GCP-R. As a result, the daytime and the dawn to dawn ratio should be different, the difference being smaller when R is small compare to GCP (autotrophy, high f ratio). On figure 9 within the errors bars, we can't estimate the difference. Nevertheless, it appears that both regimes may have prevailed at different times. This supports the choice of values of h and h*. With larger values of the MLD, the relative part of the air-sea flux in the DIC and O_2 measurements would have been smaller and make the slope of the oxygen-carbon relationship closer to 1 as in figure 8. Further, the linear distribution of the data points (figure 9) demonstrates that our technique satisfactorily identifies the biological signature during the selected periods that we have considered.

In table 2 (columns 3 and 5), we note the larger contribution of the air-sea exchange for oxygen (positive) relatively to carbon (negative), with a mean ratio of the absolute values close to 6. In the calculation of NCP_C, the contribution of CO_2 air-sea exchange is low, and varies between 7% and 25% of the measured change of DIC. By contrast, for oxygen, air-sea exchange represents 50% to 135% of the outgassing of O_2 which results in a large uncertainty in the calculation of NCP_{O2}. This situation occurs during observations made during the 11-13 December period, when it is not been possible to isolate the oxygen biological signal due to the large air-sea flux.

This is an issue regarding the in situ estimates of NCP based on dissolved oxygen argon measurements at the ocean surface (Cassar et al, 2009) in high wind regions when the air-sea flux is large. NCP based on O_2 measurements have to be considered with caution as long as the biological contribution is a small term relative to the air-sea exchange one.

Simultaneous measurements of oxygen and carbon ratios on oceanographic moorings have been reported in a few situations in tropical or mid latitudes. Lefèvre and Merlivat (2012), based on data in the tropical Atlantic Ocean on a Pirata mooring equipped with a Carioca pCO_2 sensor and an oxygen optode found an O_2/DIC ratio ranging between -1.0 and -1.3.

Johnson [2010], using simultaneous measurements of O_2 and DIC, at two moorings M1 and M2 off Monterey Bay, in California, found −0.77 ± 0.02 and ±0.93 ± 0.03 respectively for the O_2: TCO_2 ratio. He explains these low values by the different impact of gas exchange on DIC and O_2, the gas exchange for O_2 being 10 times faster than for CO_2. Martz et al (2014) use autonomous oxygen and dissolved inorganic carbon observations to examine the oxygen carbon relationship at an upwelling site in the Southern California Current System. They compute a mean value of O_2/DIC equal to - 1.20 ± 0.01 and conclude that it is in good agreement with Redfield ratio, in spite a number different of the theoretical value of the Redfield ratio, 1.30.

We think that the distribution of our observed simultaneous biological changes of DIC and O_2 (figure 9) exhibit convincingly a spectrum of values ranging from near 100% new production to 100% regenerated production regime.

4.4 Air-sea flux

A striking feature is the abrupt change of the direction of the air-sea CO_2 and O_2 fluxes, from a sink of atmospheric CO_2 at the ocean surface (the opposite for O_2) to a source, on an episodic event on November 16 and on December 16 when the buoy escapes the iron fertilized plume to enter the polar frontal zone (figure 5). It illustrates how the carbon biological pump is at first order controlled by the iron availability in the water in the plume. These observations highlight the necessity to take into consideration the limits of the different water masses in order to spatially extrapolate field measurements of CO_2 air-sea flux in highly dynamic ocean area like the Southern Ocean. This is reinforced in an iron fertilized region, as the distribution of the iron concentration is closely linked to this dynamic environment.

5 Summary and Conclusion

Hourly pCO_2 and oxygen measurements have been made along the trajectory of a CARIOCA drifter downstream from the Kerguelen plateau during the austral bloom from 1st November 2011 until 12 February 2012. From 1st November to 12 November, the buoy drifted through a cyclonic meander of the polar front, followed it eastward until 16 December, before heading north and entered the polar frontal zone .The surface water is supersaturated in oxygen until

16 December while pCO_2 ocean is smaller than pCO_2 atmosphere, suggesting that biological production dominates. North of the polar frontal zone, the ocean is a source of CO_2 for the atmosphere and a sink of oxygen.

Using an alkalinity-salinity relationship, DIC is calculated from pCO_2 and alkalinity. Net community production is calculated from changes of DIC and / or oxygen over short periods of time when biological activity is present and no mixing is encountered. NCP values obtained from 23 November to 13 December decrease from 140± 7 mmol C $m^{-2}d^{-1}$ to 60± 12 mmol C $m^{-2}d^{-1}$. Concomitant O_2 increases and DIC decreases allow the calculation of the oxygen carbon stoichiometric ratio O_2/C in organic matter (dissolved and particulate) after subtracting the contribution of CO_2 and O_2 air-sea gas exchange. O_2/C values range between 1.1 and 1.4 as expected for new and regenerated biological production regimes.

In the vicinity of the polar front, within the downstream plateau Kerguelen plume, the absorbed CO_2 air-sea flux is equal to -8mmol $m^{-2}d^{-1}$ and the O_2 outgassing equal to +38mmol $m^{-2}d^{-1}$. In the polar frontal zone from 16 December 2011 to 12 February 2012, the ocean surface is a source of CO_2 for the atmosphere equal to +5mmol$m^{-2}d^{-1}$and a sink for O_2 equal to -48mmol $m^{-2}d^{-1}$. The abrupt simultaneous changes of the sign of the air-sea CO_2 and O_2 fluxes when the buoy crosses the polar front show the dominant contribution westward in the iron fertilized Kerguelen plume of biology, which is characterised by an absorption of CO_2 and an outgassing of O_2. However a patchy distribution of iron within the plume can lead to a patchy organic carbon production and consequently affect unevenly in time and space the uptake of atmospheric CO_2. For instance, this is well illustrated when the buoy crosses the polar front on 16 December. This study points that care should be taken when extrapolating sparse air-sea flux measurements observations without an understanding of the hydrodynamic features of the upper ocean.

Acknowledgments

We are grateful to N. Martin from LOCEAN for software development and to L. Beaumont from DT-INSU, who supervised the CARIOCA preparation. We thank S. Blain, project leader, and B. Quéguiner, chief scientist, as well as the captain and crew of R.R.V. Marion Dufresne and the staff at the French Polar Institute (IPEV) who provided logistic support. Special thanks to Claire Lo Monaco for access to pCO_2 results and Dominique Lefèvre for access to O_2results. We thank Y.Park for having provided the data files for correctly positioning the polar front. We also enjoyed the stimulating discussions with N.Cassar during his stay at LOCEAN and the comments of S.Blain in the course of the preparation of the manuscript.

The research leading to these results was supported through EU FP6 project CARBOOCEAN (contract 511176) and EU FP7 project CARBOCHANGE “Changes in carbon uptake and emissions by oceans in a changing climate” which received funding from the European Commission’s Seventh Framework Program under grant agreement no.264879. The KEOPS2 project was funded by the French institutes INSU (Institut National des Sciences de l’Univers), IPEV (Institut Paul Emile Victor) and ANR (Agence Nationale de la Recherche).

References

Blain, S., Quéguiner, B., Armand, L., Belviso, S., Bombled, B.,Bopp, L., Bowie, A., Brunet, C., Brussaard, C., Carlotti, F., Christaki, U., Corbière, A., Durand, I., Ebersbach, F., Fuda, J.- L., Garcia, N., Gerringa, L., Griffiths, B., Guigue, C., Guillerm, C., Jacquet, S., Jeandel, C., Laan, P., Lefèvre, D., Lo Monaco, C., Malits, A., Mosseri, J., Obernosterer, I., Park, Y.-H., Picheral, M., Pondaven, P., Remenyi, T., Sandroni, V., Sarthou, G., Savoye, N., Scouarnec, L., Souhaut, M., Thuiller, D., Timmermans, K., Trull, T., Uitz, J., van Beek, P., Veldhuis, M., Vincent, D., Viollier, E., Vong, L. and Wagener, T. (2007) Effect of natural iron fertilization on carbon sequestration in the Southern Ocean, Nature, 446, 1070-1074, doi:10.1038/nature05700.

Blain, S., Sarthou, G., Laan, P., 2008. Distribution of dissolved iron during the natural iron fertilization experiment KEOPS (Kerguelen Plateau, Southern Ocean), *Deep Sea Research Part II: Topical Studies in Oceanography* 55, 594-605.

Borrione, I., and Schlitzer, R. (2013). Distribution and recurrence of phytoplankton blooms around South Georgia, Southern Ocean, Biogeosciences, 10, 217-231.

Boutin J., Merlivat L., Hénocq C., Martin N.,and J.B. Sallée (2008) Air-sea CO2 flux variability in frontal regions of the Southern Ocean from CARIOCA drifters, *Limnol. Oceanogr. 53: 2062-2079*

Boutin, J., and Merlivat, L. (2009). New in situ estimates of carbon biological production rates in the Southern Ocean from CARIOCA drifter measurements, *Geophys. Res. Lett.*, **36**, L13608.

Boyd, P.W., Jickells, T., Law, C.S., Blain, S., Boyle, E.A., Buesseler, K.O., Coale, K.H., Cullen, J.J., de Baar, H.J.W., Follows, M., Harvey, M., Lancelot, C., Levasseur, M., Owens, N.P.J., Pollard, R., Rivkin, R.B., Sarmiento, J., Schoemann, V., Smetacek, V., Takeda, S., Tsuda, A., Turner, S., Watson, A.J., 2007. Mesoscale iron enrichment experiments 1993-2005: Synthesis and future directions. *Science* 315, 612-617.

Cassar, N.,Barnett, B.A.,Bender,M.L., et al, (2009), Continuous high frequency dissolved O_2/Ar measurements by equilibrator inlet mass spectrometry, *Analytical Chemistry*, 81, 5, 1855-1864.

Cavagna, A.J., Fripiat, F, Elskens, M, Dehairs, F, Mangion, P, Chirurgien, L, Closset, I, Lasbleiz, M, Flores-Leiva, L, Cardinal, D, Leblanc, K, Fernandez, C, Lefèvre, D, Oriol, L, and B. Quéguiner, (2014), Biological productivity regime and associated N cycling in the surface waters over and downstream the Kerguelen Island area, Southern Ocean, Biogeosciences Discuss., 11, 18073–18104, doi:10.5194/bgd-11-18073-2014

Copin-Montegut, C. (2000), Consumption and production on scales of a few days of inorganic carbon, nitrate and oxygen by the planktonic community: results of continuous measurements at the Dyfamed Station in the northwestern Mediterranean Sea (May 1995), *Deep-Sea Research I,* 47, 447-477.

Dickson, A.G., and Millero, F.J. (1987), A comparison of the equilibrium constants for the dissociation of carbonic acid in seawater media. *Deep-Sea Res.*, **34**, 1733-1743.

d'Ovidio, F., et al. (2015), The biogeochemical structuring role of horizontal stirring: Lagrangian perspectives on iron delivery downstream of the Kerguelen plateau, Biogeosciences Discuss., 12, 779–814, doi:10.5194/bgd-12-779-2015

Friedlingstein, P., et al. (2006), Climate-carbon cycle feedback analysis: Results from the (CMIP)-M-4 model intercomparison, Journal of Climate, 19(14), 3337-3353.

Garcia, H.E., and Gordon, L.I. (1992), Oxygen solubility in seawater: better fitting equations. *Limnol. Oceanogr.*, **37 (6)**, 1307-1312.

Gruber, N., et al. (2009), Oceanic sources, sinks, and transport of atmospheric CO_2, *Global Biogeochem. Cycles*, 23. GB1005, doi:10. 1029/2008GB003349.

Hood, E.M. and L. Merlivat, Annual to interannual variations of fCO2 in the northwestern Mediterranean Sea: high frequency time series data from CARIOCA buoys (1995-1997), *Journal of Marine Research* , 59, 113-131, 2001

Johnson, K. S. (2010), Simultaneous measurements of nitrate, oxygen, and carbon dioxide on oceanographic moorings: Observing the Redfield ratio in real time, *Limnol. Oceanogr.,* 55(2), 615–627, doi:10.4319/lo.2009.55.2.0615.

Jouandet et al. (2008), A seasonal carbon budget for a naturally iron-fertilized bloom over the Kerguelen Plateau in the Southern Ocean, *Deep-Sea Research II,* 55, 856–867.

Laws, E. A. (1991), Photosynthetic quotients, new production and net community production in the open ocean, *Deep Sea Research,* 38, 143–167, doi:10.1016/0198-0149(91)90059-O.

Lefevre, D., Guigue, C., Obernosterer, I., (2008). The metabolic balance at two contrasting sites in the Southern Ocean: The iron-fertilized Kerguelen area and HNLC waters. *Deep-Sea Research* II, 55 ,766–776

Lefèvre, N., and L. Merlivat (2012), Carbon and oxygen net community production in the eastern tropical Atlantic estimated from a moored buoy, *Global Biogeochem. Cycles*, *26*, GB 1009, doi: 10. 1029/2010 GB004018.

Lenton A., B. Tilbrook, R. M. Law, D. Bakker, S. C. Doney, N. Gruber, M. Ishii, M. Hoppema, N. S. Lovenduski, R. J. Matear, B. I. McNeil, N. Metzl, S. E. Mikaloff Fletcher, P. M. S. Monteiro, C. Rödenbeck, C. Sweeney, and T. Takahashi. (2013), Sea-air CO_2 fluxes in the Southern Ocean for the period 1990–2009, *Biogeosciences*, 10, 4037-4054, doi: 10.5194/bg-10-4037-2013 .

Le Quere, C., T. Takahashi, E. T. Buitenhuis, C. Rodenbeck, and S. C. Sutherland (2010), Impact of climate change on the global oceanic sink of CO_2, Global Biogeochem. Cycles, doi: 10.1029/2009GB003599.

Lo Monaco, C., Metzl, N., d'Ovidio, F., Llort, J., and C. Ridame (2014), Rapid establishment of the CO_2 sink associated with Kerguelen's bloom observed during the

KEOPS2/OISO20 cruise, Biogeosciences Discuss., 11, 17543–17578, doi:10.5194/bgd-11-17543-2014

Martz, T., U. Send, M. D. Ohman, Y.Takeshita, P. Bresnahan, H.-J. Kim, and S.H. Nam (2014), Dynamic variability of biogeochemical ratios in the Southern California Current System, *Geophys. Res.Lett.,* 41, 2496–2501, doi:10.1002/ 2014GL059332.

Mehrbach, C., Culberson, C.H., Hawley, J.E., and Pytkowicz, R.M. (1973), Measurement of the apparent dissociation constants of carbonic acid in seawater at atmospheric pressure. *Limnol. Oceanogr.*, **18**, 897-907.

Merlivat, L., M. Gonzales-Davila, G. Caniaux, J. Boutin, and G. Reverdin, (2009), Mesoscale and diel to monthly variability of CO2 and carbon fluxes at the ocean surface in the northeastern Atlantic, *J. Geophys. Res., 114*, C03010, doi:10.1029/2007JC004657.

Merlivat, L., Boutin, J., Antoine, D., (2014) Roles of biological and physical processes in driving seasonal air-sea CO_2 flux in the Southern Ocean: New insights from CARIOCA pCO_2, *J. Mar. Syst*., http://dx.doi.org/10.1016/j.jmarsys.2014.04.015

Metzl, N., B. Tilbrook, and A. Poisson (1999), The annual fCO_2 cycle and the air-sea CO2 flux in the sub-Antarctic Ocean, Tellus Series B-Chemical and Physical Meteorology, 51(4), 849-861

Park, Y.-H., F. Vivier, F. Roquet, and E. Kestenare (2009), Direct observations of the ACC transport across the Kerguelen Plateau, *Geophys. Res. Lett.,* 36, L18603, doi: 10.1029/2009GL039617.

Park, Y.-H., and F. Vivier (2011), Circulation and hydrography over the Kerguelen Plateau, in *The Kerguelen Plateau: marine ecosystem and fisheries*, edited by G. Duhamel et al., pp.597 43-55, Cybium, Paris.

Park, Y.-H., I. Durand, E. Kestenare, G. Rougier, M. Zhou, F. d'Ovidio, C. Cotté, J.-H. Lee

(2014), Polar Front around the Kerguelen Islands: An up-to-date determination and associated circulation of surface/subsurface waters, *J. Geophys. Res.,* doi: 10. 1002/2014JC010061.

Pollard, R.T., Salter, I., Sanders, R.J., Lucas, M.I., Moore, C.M., Mills, R.A., Statham, P.J., Allen, J.T., Baker, A.R., Bakker, D.C.E., Charette, M.A., Fielding, S., Fones, G.R., French, M., Hickman, A.E., Holland, R.J., Hughes, J.A., Jickells, T.D., Lampitt, R.S., Morris, P.J., Nedelec, F.H., Nielsdottir, M., Planquette, H., Popova, E.E., Poulton, A.J., Read, J.F., Seeyave, S., Smith, T., Stinchcombe, M., Taylor, S., Thomalla, S., Venables, H.J., Williamson, R., Zubkov, M.V., 2009. Southern Ocean deep-water carbon export enhanced by natural iron fertilization, *Nature* 457, 577-580.

Stanley, R. H. R., W. J. Jenkins, D. E. Lott III, and S. C. Doney (2009), Noble gas constraints on air-sea gas exchange and bubble fluxes, *J. Geophys. Res.*, 114, C11020, doi: 10.1029/2009JC005396

Sweeney, C., Gloor, E., Jacobson, A.R., Key, R.M., McKinley, G., Sarmiento, J.L., and Wanninkhof, R. (2007), Constraining global air-sea gas exchange for CO_2 with recent bomb ^{14}C measurements. *Global Biogeochem. Cycles*, **21**, doi: 10.1029/2006GB002784.

Takahashi, T., et al. (2009), Climatological mean and decadal change in surface ocean pCO(2), and net sea-air CO_2 flux over the global oceans, Deep-Sea Research Part Ii-Topical Studies in Oceanography, 56(8-10), 554-577.

Taylor, J.R and Ferrari, R. (2011), Ocean fronts trigger high latitude phytoplankton blooms. *Geophys. Res. Lett.*, 38, L23601, doi:10.1029/2011GL049312.

Trull,T.W., Davies, D. M., Dehairs, F., Cavagna,A.J., Lasbleiz, M., Laurenceau,E.C., d'Ovidio, F., Planchon,F., Leblanc, K., Quéguiner,B., and S. Blain, (2015), Chemometric perspectives on plankton community responses to natural iron fertilization over and downstream of the Kerguelen plateau in the Southern Ocean, *Biogeosciences* 12, 1029-1056, doi:10.5194/bg-12-1029-2015

Wanninkhof, R.H. (1992), Relationship between wind speed and gas exchange over the ocean. *J. Geophys. Res.*, **97 (C5)**, 7373-7382.

Weiss, R.F. (1974), CO_2 in water and seawater: the solubility of a non-ideal gas. *Mar. Chem.*, **2**, 203-215.

Woolf, D.K., and Thorpe, S.A. (1991), Bubbles and the air-sea exchange of gases in near-saturation conditions. *J. Mar. Res.*, **49**, 435-466.

Table 1. Difference between the extrema of DIC and O_2 measured in the warm surface layer (columns 4 and 6). In bold, mean values of DIC and O_2 changes over consecutive mornings (columns 5 and 7), CO_2 and O_2 air-sea flux (columns 8 and 9).

Date	Latitude Longitude	SST °C	DIC_{min}-DIC_{max} µmol kg^{-1}	$dDIC_{max}/dt$ µmol kg^{-1}	O_{2max}-O_{2min} µmol kg^{-1}	dO_{2min}/dt µmol kg^{-1}	F_{CO2} mmol m^{-2} d^{-1}	F_{O2} mmolm^{-2}d^{-1}
1	2	3	4	5	6	7	8	9
18 Nov	49.3°S76.4°E	4.2	-6.46±1.00		7.19±1.00			
23-25 Nov	**50.1°S77°4E**	**4.3**		**-4.72±0.23**		**3.74±0.54**	**-8.21**	**42.9**
23 Nov			-11.50±1.00		9.77±1.00			
24 Nov			-10.09±1.00		11.41±1.00			
26-28 Nov	**50.4°S77.3°E**	**4.4**		**-4.22±0.85**		**3.90±1.01**	**-5.83**	**38.5**
27 Nov			-9.35±1.00		8.39±1.00			
30Nov4Dec	**50.4°S79.8°E**	**4.5**		**-1.76±0.43**		**1.71±0.32**	**-9.13**	**47.4**
30 Nov			-8.50±1.00		6.17±1.00			
1 Dec			-5.79±1.00		5.73±1.00			
2 Dec			-7.80±1.00		7.25±1.00			
11-13 Dec	**50.2°S81.4°E**	**4.6**		**-2.10±0.65**			**-10.49**	**61.0**

Table 2. Biological changes (columns 2 and 4) and air-sea flux changes (columns 3 and 5) of DIC and O_2. In bold, mean values over consecutive mornings. Calculated values of NCP carbon and NCP oxygen (columns 6 and 7)

Date	$dDIC_{bio}$	$dDIC_{air\text{-}sea}$	dO_{2bio}	$dO_{2\ air\text{-}sea}$	NCP_C	NCP_{O2}
	μmol kg^{-1}	μmol kg^{-1}	μmol kg^{-1}	μmol kg^{-1}	mmol C $m^{-2}d^{-1}$	mmol O_2 $m^{-2}d^{-1}$
1	2	3	4	5	6	7
18 Nov	-6.79±1.00	-0.32±0.10	10.23±1.35	3.03±0.91		
23-25 Nov	**-5.12±0.26**	**-0.40±0.12**	**5.83±0.83**	**2.09±0.63**	**-140±7**	**160±23**
23 Nov	-12.43±1.04	-0.93±0.28	14.18±1.66	4.41±1.32		
24 Nov	-10.47±1.00	-0.38±0.11	13.88±1.24	2.47±0.74		
26-28 Nov	**-4.50±0.85**	**-0.28±0.09**	**5.78±1.16**	**1.87±0.56**	**-124±23**	**159±31**
27 Nov	-9.74±1.01	-0.39±0.12	10.85±1.24	2.46±0.74		
30Nov4Dec	**-2.20±0.45**	**-0.44±0.13**	**4.02±0.76**	**2.31±0.69**	**-60±12**	**111±20**
30 Nov	-9.07±1.01	-0.58±0.17	8.78±1.27	2.60±0.78		
1 Dec	-6.44±1.02	-0.66±0.20	9.78±1.57	4.05±1.22		
2 Dec	-8.38±1.02	-0.58±0.17	10.88±1.48	3.63±1.09		
11-13 Dec	**-2.61±0.67**	**-0.51±0.15**		**2.96±0.89**	**-72±17**	

FIGURE CAPTIONS

Figure 1. Trajectory followed by the Carioca drifter from 1 November 2011 to 12 February 2012 (red line). The green dots and letters indicate the location and time where the data indicate a large signature of biological effects. The grey diamonds indicate high isolated salinity anomalies. The buoy enters the polar frontal zone at the location of the blue arrow. The pink dotted line represents the location of the subantarctic front, SAF, the blue dashed line shows the location of the polar front (Park et al, 2009, 2011) and the black line, the location of the polar front based on KEOPS 2 observations, PF_Park, (Park et al,2014). The black dots indicate the location of the KEOPS 2 stations,TEW-7,TEW-8,NPF-L, close to the PF.

Figure 2. Diurnal cycles of SST, DIC and O_2 from 30 November to 4 December 2011. **a** SST (°C) (black, left vertical axis) and DIC (µmol kg^{-1}) (grey, right vertical axis).The vertical dashed lines indicate the time of sunrise (blue) and sunset (orange). **b** O_2 (µmol kg^{-1}) (black, left vertical axis) and DIC (grey, right vertical axis).

Figure 3. Spatial extent of phytoplankton blooms over and downstream from the Kerguelen plateau as revealed by satellite ocean color on 6 selected days, from 11 November to 28 December 2011. The trajectory followed by the CARIOCA drifter is superposed on the chlorophyll patches (black line). The circles indicate the location of the buoy the same days.

Figure 4. Lagrangian perspectives on large scale natural iron fertilization on the Kerguelen plateau and in the downstream plume: a snapshot on 25 November 2011.The color code indicates the time in days since leaving the plateau for each water parcel (d'Ovidio et al, 2015). The white line indicates the trajectory of the Carioca drifter from 1 November to 31 December 2011.The cyan dots indicate the locations where carbon NCP estimates are calculated. The cyan square is the position of the buoy on 16 November (see text).

Figure 5. Buoy data from 1 November 2011 to 12 February 2012. **a** temperature in °C (black, left vertical axis) and salinity (grey, right vertical axis). **b** T-S diagram: 1 to 11 November, black diamonds- 12 November to 16 December, grey diamonds- 17 December to 12 February, black squares. **c** pCO2 measured at a depth of 2 meters in µatm (black) and in the atmosphere in µatm (grey). **d** Dissolved oxygen concentration measured at a depth of 2 meters in µmol kg^{-1}(black, left vertical axis) and oxygen saturation in % (grey, right vertical axis). In figure 5a, the cyan dashed lines indicate the 12 November and 16 December days (see text). In figure 5b,the red dots indicate the data measured at the KEOPS 2 stations, TEW7, TEW8, F-L.

Figure 6. Air-sea flux from 1 November 2011 to 12 February 2012 in mmol $m^{-2}d^{-1}$ (positive for outgassing). **a** O_2). **b** CO_2

Figure 7. Distribution of O_2 in µmol kg^{-1} (black, left vertical axis) and DIC in in µmol kg^{-1} (grey, right vertical axis) between 1 November 2011 and 12 February 2012. The purple dots and lines indicate the periods when NCP estimates have been made. The cyan dashed lines indicates the 12 November and 16 December days and the cyan arrow the 16 November (see text).

Figure 8. Measured changes (absolute values) of O_2 (µmol kg^{-1}) as a function of measured changes (absolute values) of DIC (µmol kg^{-1}) between consecutive mornings, (dark blue dots), or during the daylight period (light blue dots). The slope of the black dotted line is 1.

Figure 9. Changes (absolute values) of O_2 (µmol kg^{-1}) attributed to biological activity as a function of changes (absolute values) of DIC (µmol kg^{-1}) attributed to biological activity between consecutive mornings (red dots), or during the daylight period (blue dots). The two dotted lines with a slope of 1.4 and 1.1 respectively characterize the new and regenerated production regime

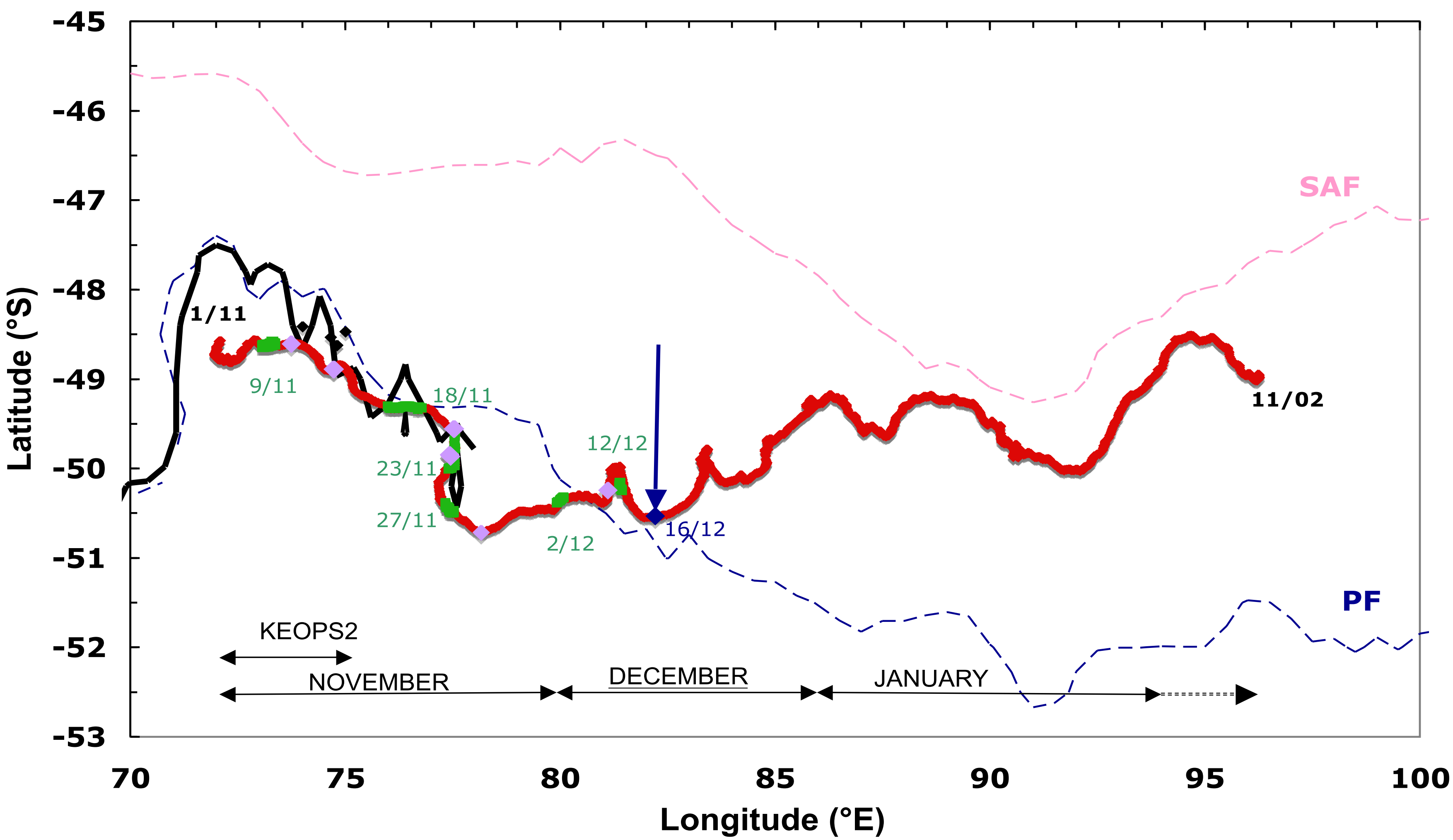
-45
-46
-47
-48
-49
-50
-51
-52
-53
Latitude (°S)
70
75
80
85
90
95
100
Longitude (°E)
SAF
PF
1/11
9/11
18/11
23/11
27/11
2/12
12/12
16/12
11/02
KEOPS2
NOVEMBER
DECEMBER
JANUARY

Figure 1

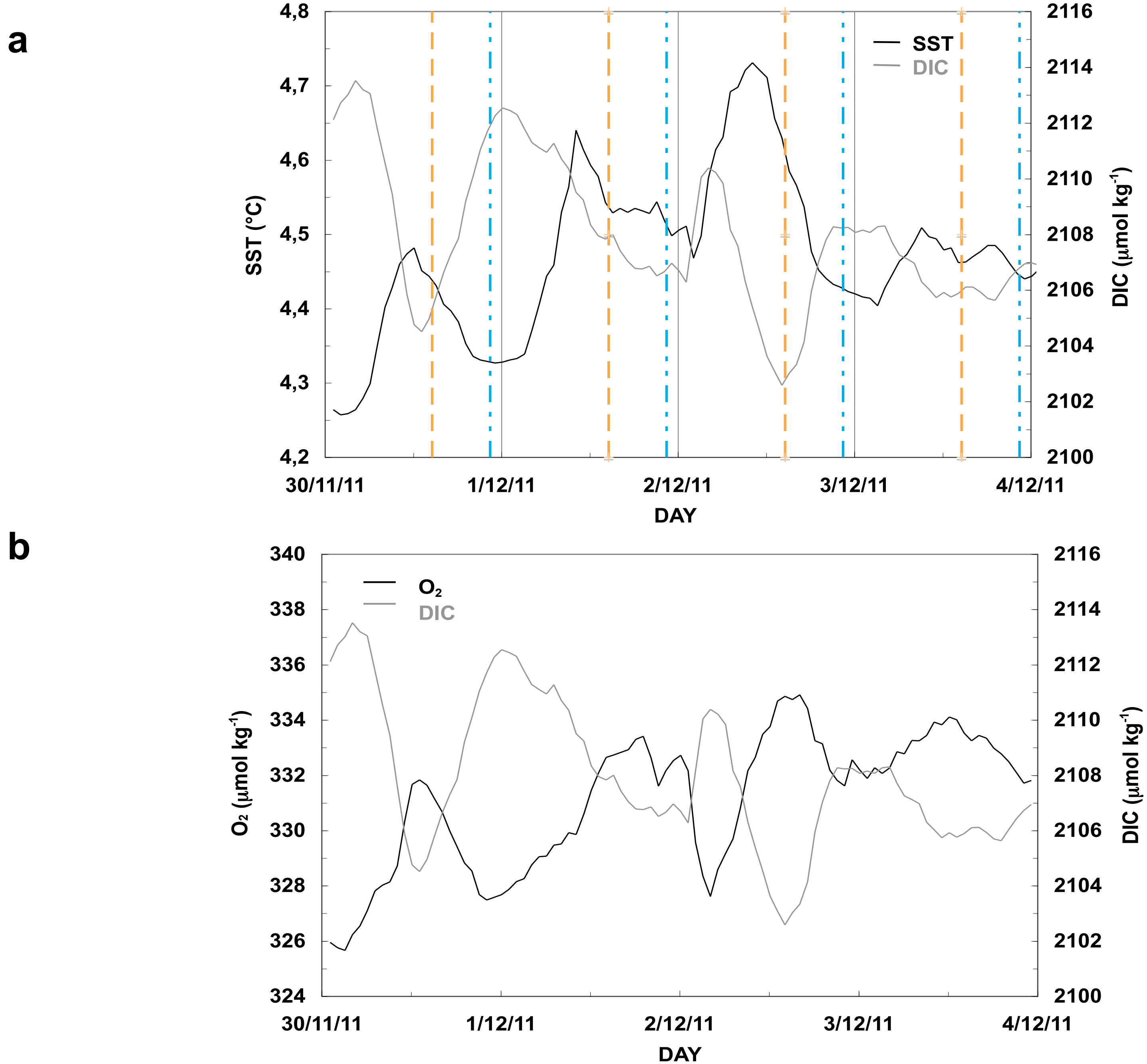
a
4,8
4,7
4,6
4,5
4,4
4,3
4,2
SST (°C)
2116
2114
2112
2110
2108
2106
2104
2102
2100
DIC (μmol kg-1)
SST
DIC
30/11/11
1/12/11
2/12/11
3/12/11
4/12/11
DAY
b
340
338
336
334
332
330
328
326
324
O2 (μmol kg-1)
2116
2114
2112
2110
2108
2106
2104
2102
2100
DIC (μmol kg-1)
O2
DIC
30/11/11
1/12/11
2/12/11
3/12/11
4/12/11
DAY

Figure 2

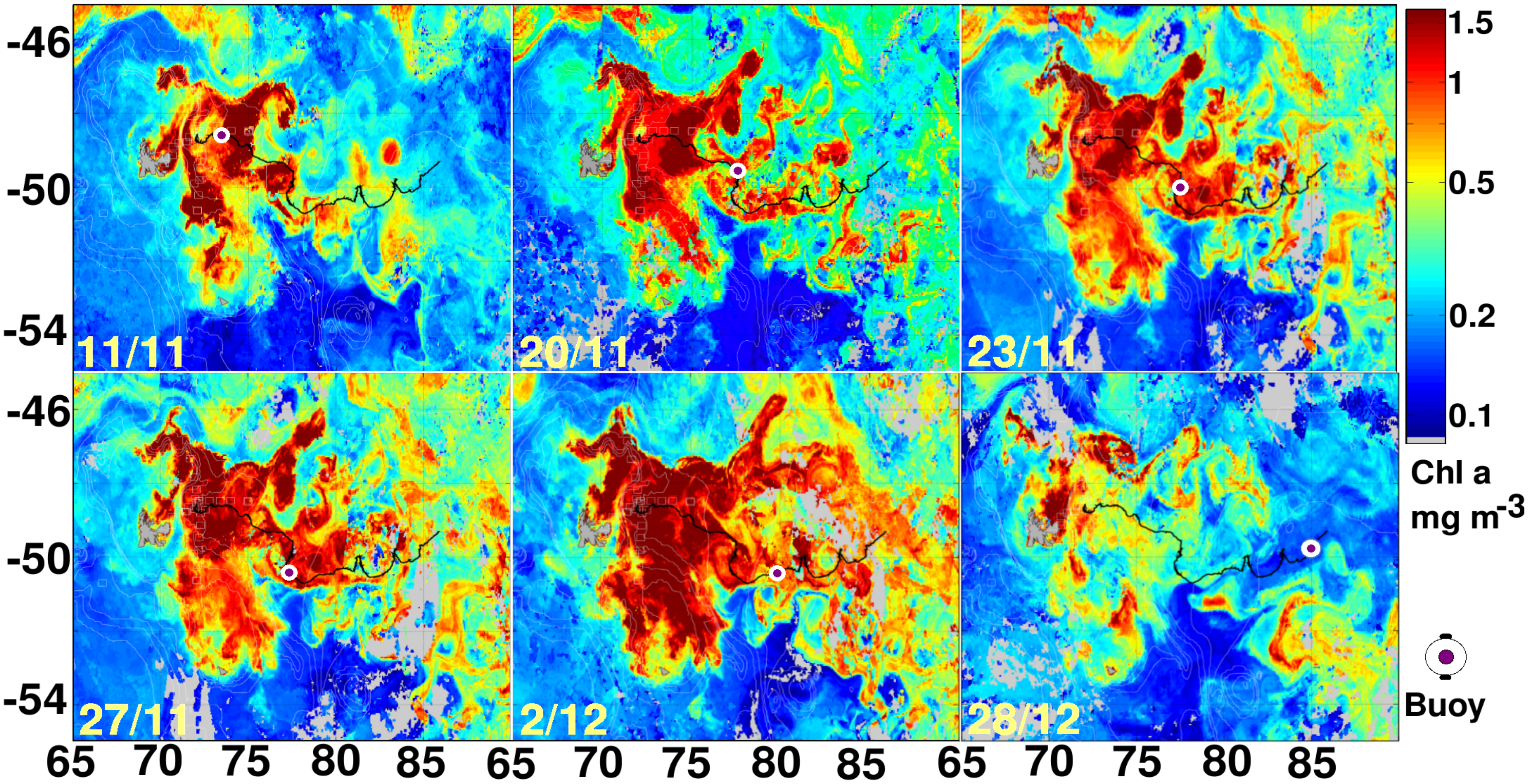
-46
-50
-54
11/11
20/11
23/11
27/11
2/12
28/12
65
70
75
80
85
1.5
1
0.5
0.2
0.1
Chl a
mg m-3
Buoy

Figure 3

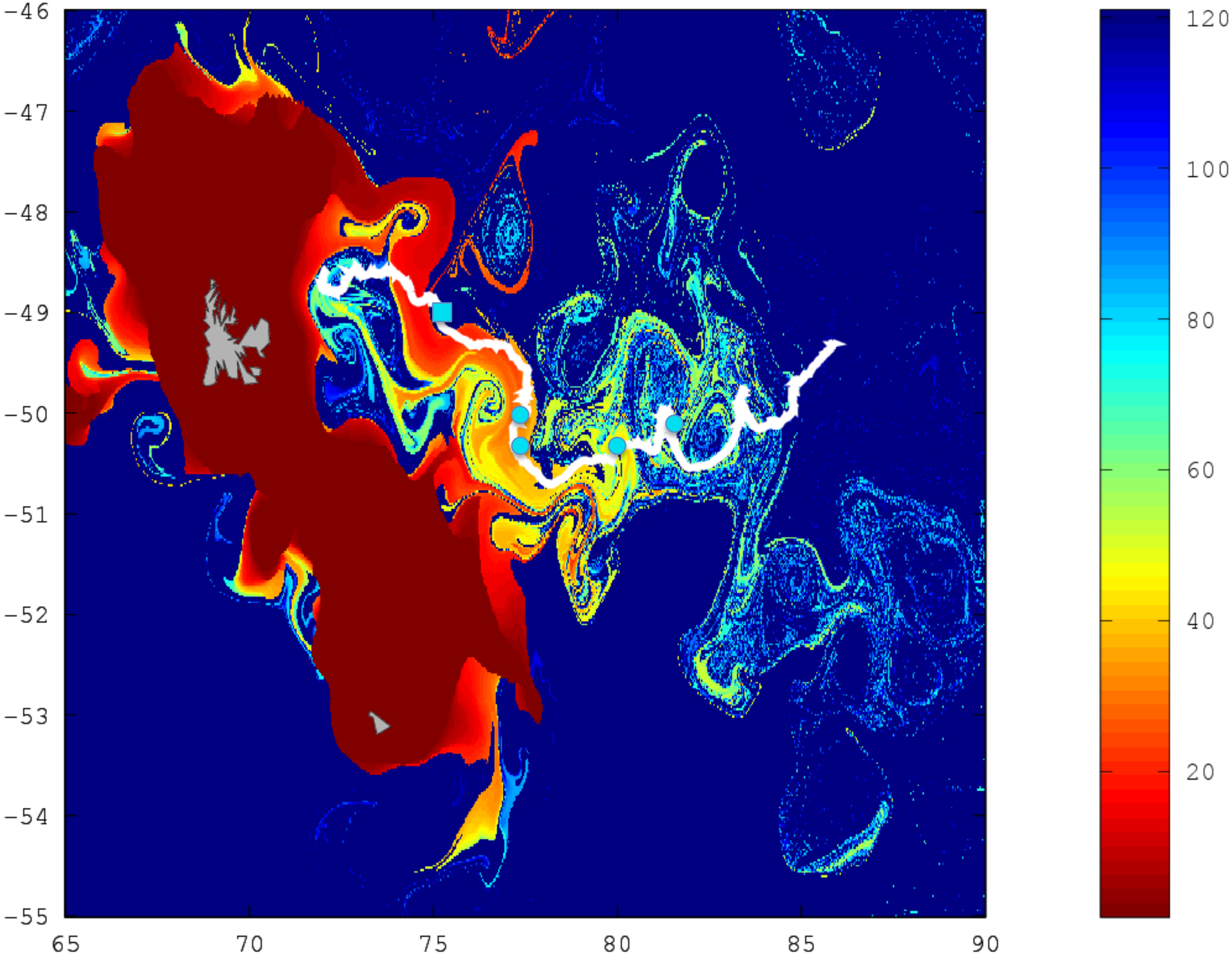

Figure 4

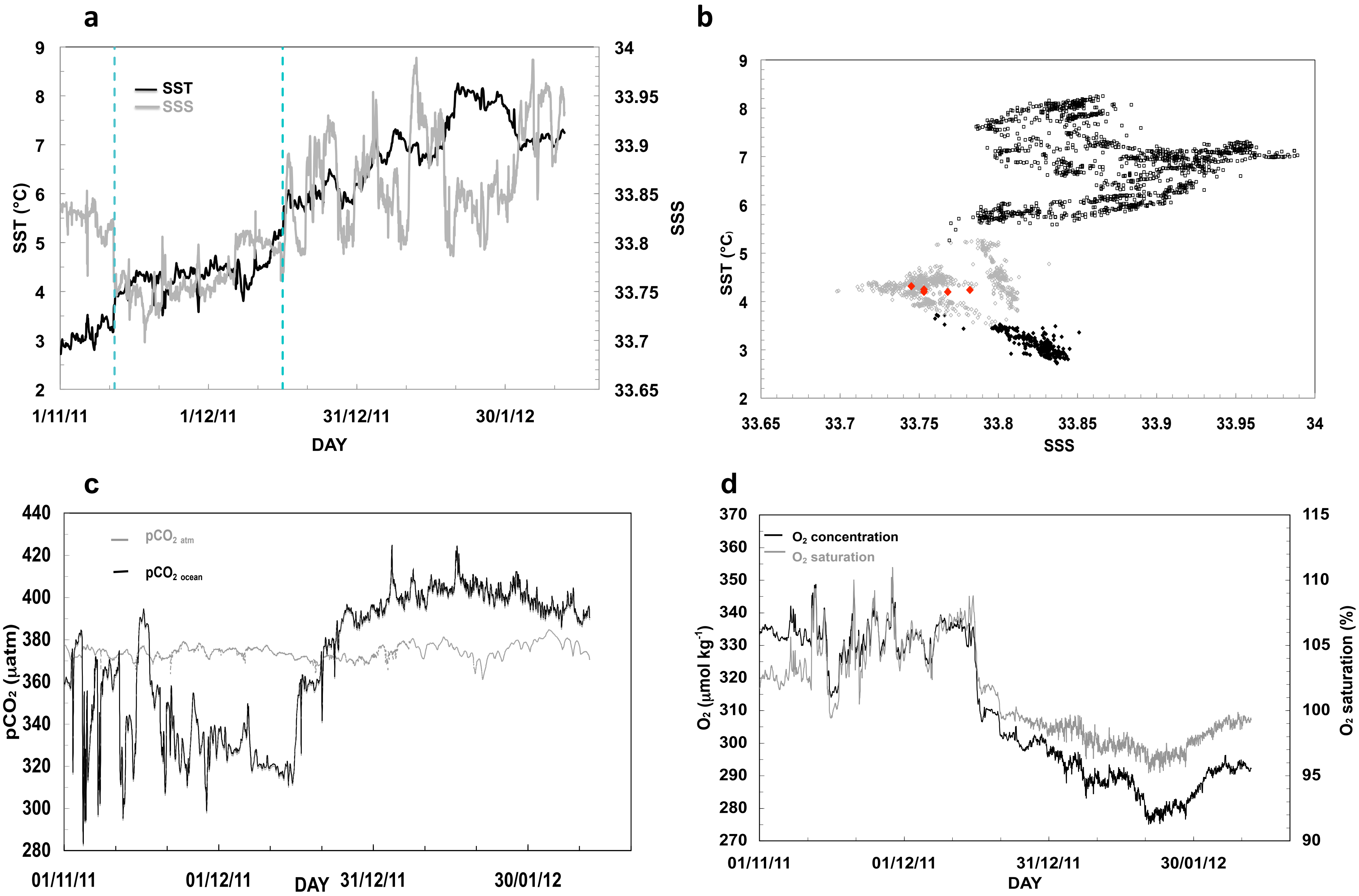
a
SST
SSS
SST (°C)
SSS
1/11/11
1/12/11
31/12/11
30/1/12
DAY
b
SST (°C)
SSS
c
pCO2 atm
pCO2 ocean
pCO2 (μatm)
01/11/11
01/12/11
31/12/11
30/01/12
DAY
d
O2 concentration
O2 saturation
O2 (μmol kg-1)
O2 saturation (%)
01/11/11
01/12/11
31/12/11
30/01/12
DAY

Figure 5

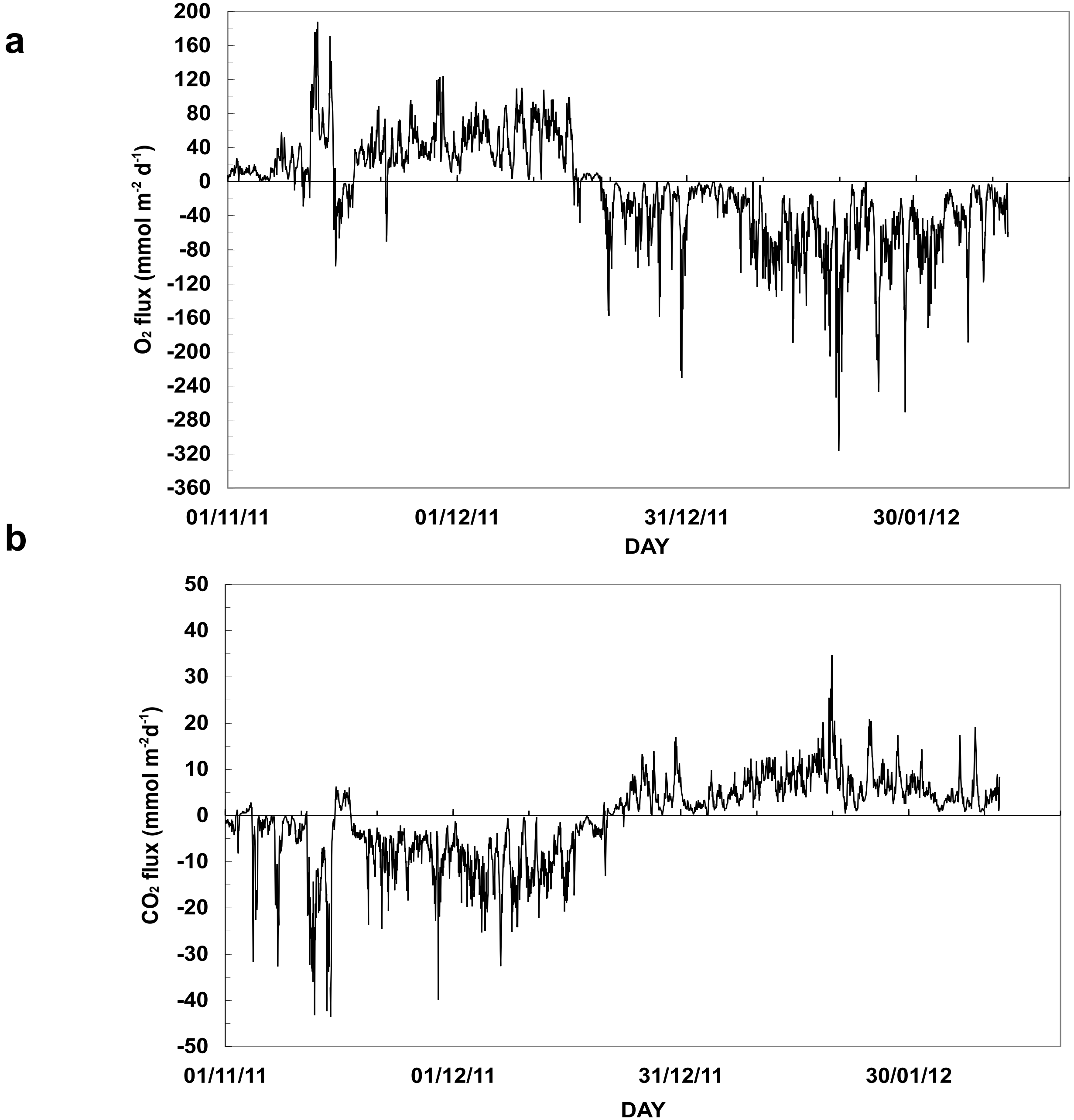
a
200
160
120
80
40
0
-40
-80
-120
-160
-200
-240
-280
-320
-360
O2 flux (mmol m-2 d-1)
01/11/11
01/12/11
31/12/11
30/01/12
DAY
b
50
40
30
20
10
0
-10
-20
-30
-40
-50
CO2 flux (mmol m-2 d-1)
01/11/11
01/12/11
31/12/11
30/01/12
DAY

Figure 6

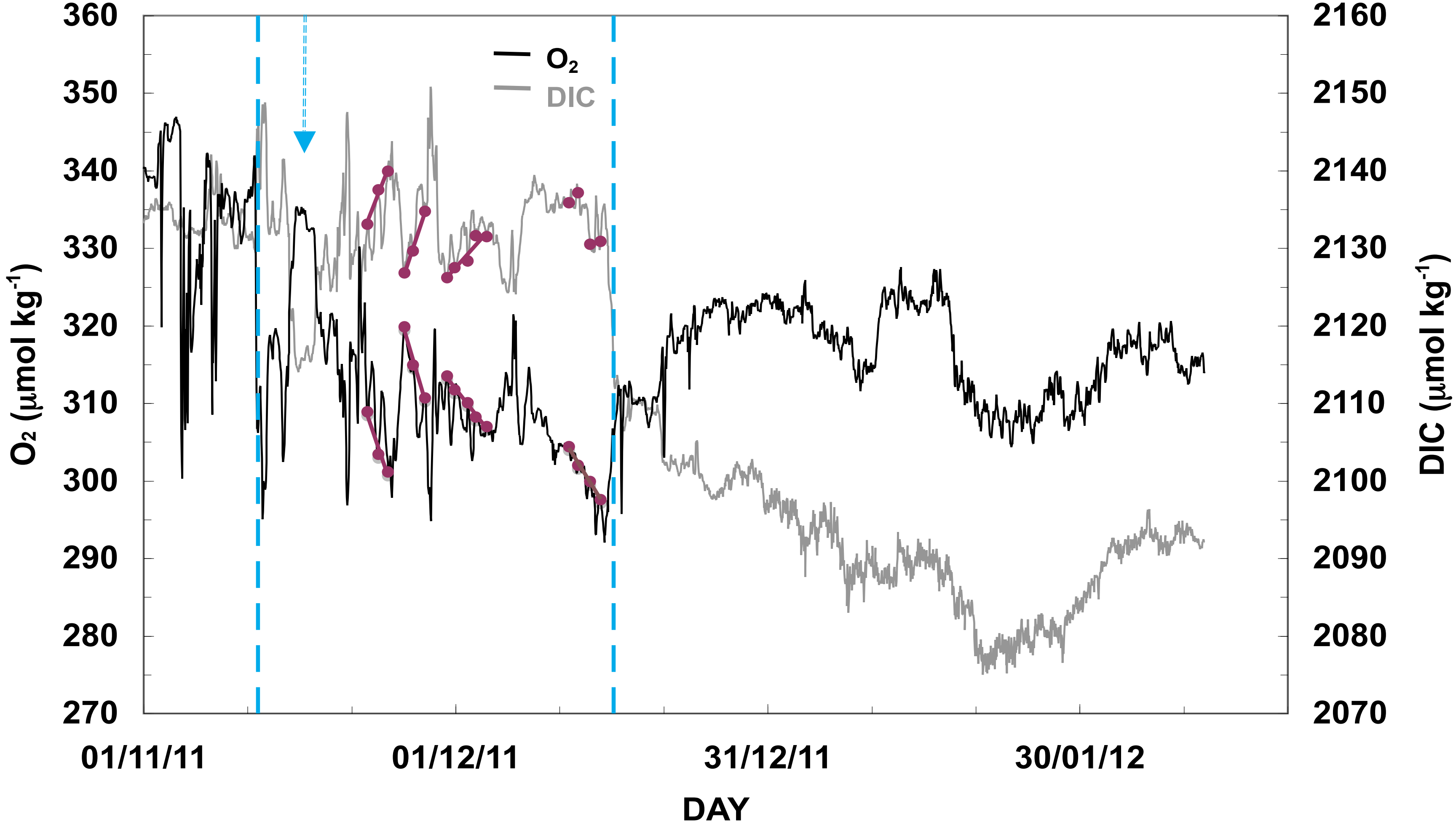

O₂
DIC
360
350
340
330
320
310
300
290
280
270
2160
2150
2140
2130
2120
2110
2100
2090
2080
2070
O₂ (µmol kg-1)
DIC (µmol kg-1)
01/11/11
01/12/11
31/12/11
30/01/12
DAY

Figure 7

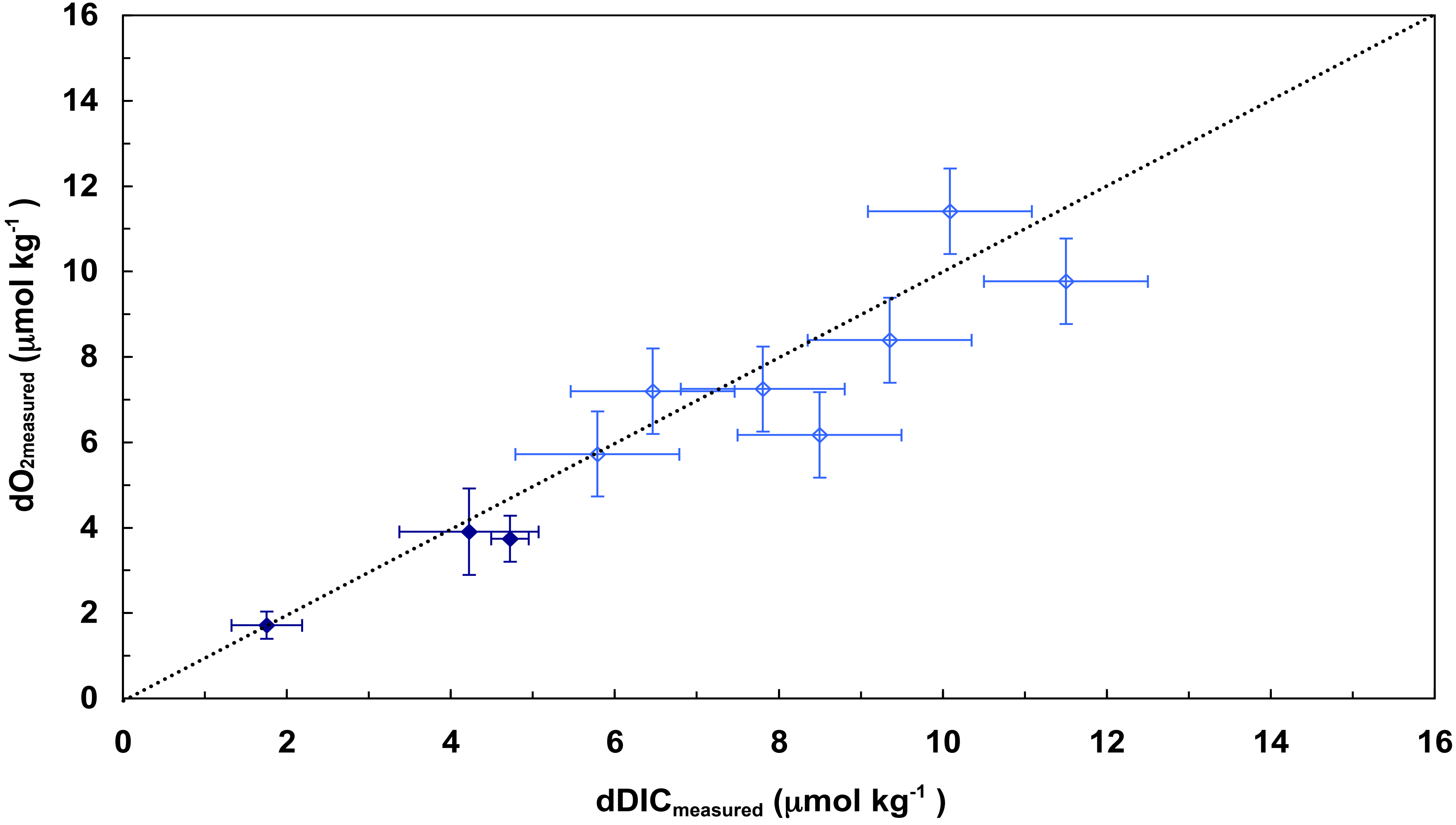
16
14
12
10
8
6
4
2
0
dO2measured (µmol kg-1)
0
2
4
6
8
10
12
14
16
dDICmeasured (µmol kg-1)

Figure 8

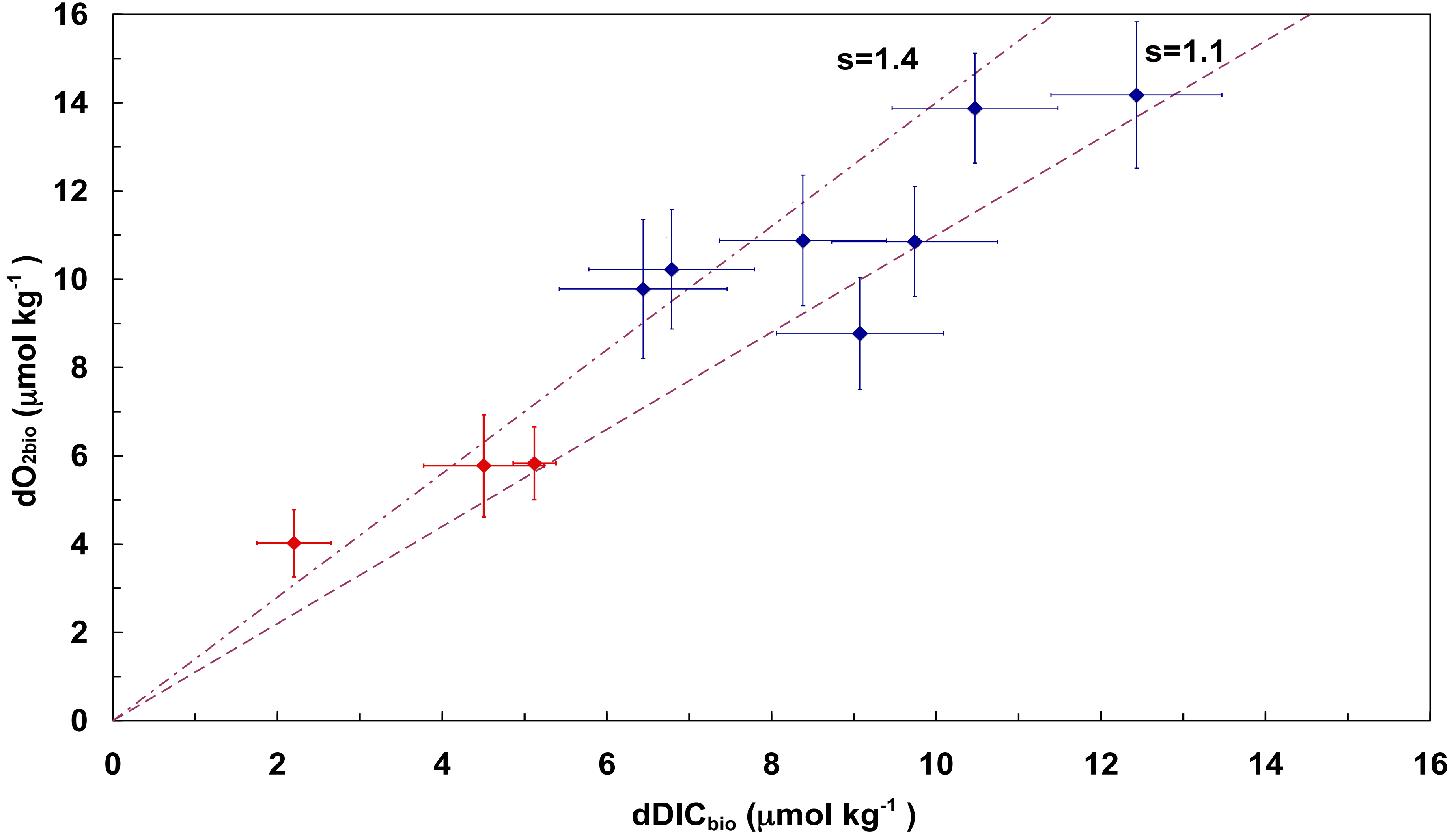

16
14
12
10
8
6
4
2
0
0
2
4
6
8
10
12
14
16
s=1.4
s=1.1
dO2bio (μmol kg-1)
dDICbio (μmol kg-1)

Figure 9